NASA/TM-2002-211668

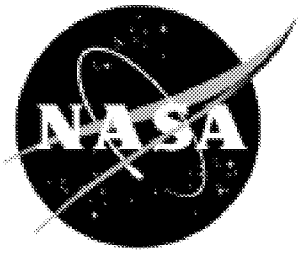

Natural and Induced Environment in Low Earth Orbit

John W. Wilson
Langley Research Center, Hampton, Virginia

Francis F. Badavi
Christopher Newport University, Newport News, Virginia

Myung-Hee Y. Kim
College of William and Mary, Williamsburg, Virginia

Martha S. Clowdsley and John H. Heinbockel
Old Dominion University, Norfolk, Virginia

Francis A. Cucinotta and Gautam D. Badhwar
Johnson Space Center, Houston, Texas

William Atwell
Boeing Company, Houston, Texas

Stuart L. Huston
Boeing Company, Huntington Beach, California

May 2002

The NASA STI Program Office . . . in Profile

Since its founding, NASA has been dedicated to the advancement of aeronautics and space science. The NASA Scientific and Technical Information (STI) Program Office plays a key part in helping NASA maintain this important role.

The NASA STI Program Office is operated by Langley Research Center, the lead center for NASA's scientific and technical information. The NASA STI Program Office provides access to the NASA STI Database, the largest collection of aeronautical and space science STI in the world. The Program Office is also NASA's institutional mechanism for disseminating the results of its research and development activities. These results are published by NASA in the NASA STI Report Series, which includes the following report types:

- TECHNICAL PUBLICATION. Reports of completed research or a major significant phase of research that present the results of NASA programs and include extensive data or theoretical analysis. Includes compilations of significant scientific and technical data and information deemed to be of continuing reference value. NASA counterpart of peer-reviewed formal professional papers, but having less stringent limitations on manuscript length and extent of graphic presentations.

- TECHNICAL MEMORANDUM. Scientific and technical findings that are preliminary or of specialized interest, e.g., quick release reports, working papers, and bibliographies that contain minimal annotation. Does not contain extensive analysis.

- CONTRACTOR REPORT. Scientific and technical findings by NASA-sponsored contractors and grantees.

- CONFERENCE PUBLICATION. Collected papers from scientific and technical conferences, symposia, seminars, or other meetings sponsored or co-sponsored by NASA.

- SPECIAL PUBLICATION. Scientific, technical, or historical information from NASA programs, projects, and missions, often concerned with subjects having substantial public interest.

TECHNICAL TRANSLATION. English-language translations of foreign scientific and technical material pertinent to NASA's mission.

Specialized services that complement the STI Program Office's diverse offerings include creating custom thesauri, building customized databases, organizing and publishing research results . . . even providing videos.

For more information about the NASA STI Program Office, see the following:

- Access the NASA STI Program Home Page at ***http://www.sti.nasa.gov***

- Email your question via the Internet to help@sti.nasa.gov

- Fax your question to the NASA STI Help Desk at (301) 621-0134

- Telephone the NASA STI Help Desk at (301) 621-0390

- Write to:
  NASA STI Help Desk
  NASA Center for AeroSpace Information
  7121 Standard Drive
  Hanover, MD 21076-1320

NASA/TM-2002-211668

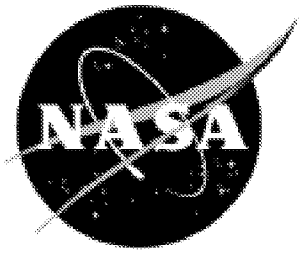

Natural and Induced Environment in Low Earth Orbit

John W. Wilson
Langley Research Center, Hampton, Virginia

Francis F. Badavi
Christopher Newport University, Newport News, Virginia

Myung-Hee Y. Kim
College of William and Mary, Williamsburg, Virginia

Martha S. Clowdsley and John H. Heinbockel
Old Dominion University, Norfolk, Virginia

Francis A. Cucinotta and Gautam D. Badhwar
Johnson Space Center, Houston, Texas

William Atwell
Boeing Company, Houston, Texas

Stuart L. Huston
Boeing Company, Huntington Beach, California

National Aeronautics and
Space Administration

Langley Research Center
Hampton, Virginia 23681-2199

May 2002

Available from:

NASA Center for AeroSpace Information (CASI)
7121 Standard Drive
Hanover, MD 21076-1320
(301) 621-0390

National Technical Information Service (NTIS)
5285 Port Royal Road
Springfield, VA 22161-2171
(703) 605-6000

Abstract

Estimating the long-term exposure of astronauts on the developing International Space Station (ISS) requires an accurate knowledge of the internal exposure environment for human risk assessment and other onboard processes. The natural environment is moderated by the solar wind, which varies over the solar cycle. The neutron environment within the Shuttle in low Earth orbit has two sources. A time dependent model for the ambient environment is used to evaluate the natural and induced environment. The induced neutron environment is evaluated using measurements on STS-31 and STS-36 near the 1990 solar maximum.

Introduction

The commitment of astronauts to long-term exposure to the space environment on the International Space Station (ISS) requires resolution of issues concerning ionizing radiation. For the high inclination of the ISS (51.6°), computational models indicate that about half of the ionizing radiation exposure near solar minimum results from Galactic Cosmic Rays (GCR, 233 μSv/d), and the bulk of the remainder is from trapped particles (166 μSv/d, Wu et al. 1996). There are, of course, contributions from the neutron albedo of 25 to 54 μSv/d (varies with solar cycle) excluding effects of intervening material (Wilson et al. 1989). Within the craft, the environment is a complex mixture of surviving primary particles and secondary radiations produced in the spacecraft structure. Various arrangements of detectors have been used to study the composition of the internal radiation fields within the spacecraft which need to be understood in terms of computational models to allow a better understanding of the local environment of the astronauts' critical tissues. As a result, a number of studies of the low Earth orbit (LEO) environment have been made to better understand the nature of the radiations within a spacecraft (Dudkin et al. 1992; Keith et al. 1992; Badhwar et al. 1995a; and Dudkin et al. 1995) and to understand these results in terms of computational models (Badhwar et al. 1995b; Shinn et al. 1995; and Shinn et al. 1998).

Measurements of neutrons on Cosmos-2044, flown at an 82° inclination between 216–296 km, resulted in 35 μSv/d using nuclear emulsion (Dudkin et al. 1992) and compares favorably with the neutron albedo model of 25 μSv/d estimated for near polar orbits at the cycle 20 solar minimum (Wilson et al. 1989). Similar measurements within the Spacehab on STS-57 in a 28.5° inclination orbit at 462 km yield 174 μSv/d compared to 12.5 μSv/d from the albedo neutrons near solar maximum. Unlike the Cosmos-2044 spacecraft, the Shuttle is itself a strong source of neutrons, especially within the massive Spacehab module in the Shuttle bay. Indeed, time-resolved neutron measurements on the Mir and Salyut stations (Lobakov et al. 1992) reveal strong neutron levels, mainly within the South Atlantic Anomaly (SAA) passage through the trapped proton belt against a lower background of neutrons in the remainder of time outside the SAA.

Neutron measurements using Bonner spheres and gold foils were made (Keith et al. 1992) near solar maximum in the low inclination (28.5°) with high altitude (617 km) flight STS-31 in April 1990 and in the high inclination (62°) with low altitude (246 km) flight STS-36 in February 1990. The neutron dose equivalent on STS-36 was found to be 45 μSv/d compared to 25 μSv/d from the albedo model, and on STS-31 the measurements were 345 μSv/d compared to 12.5 μSv/d from the albedo model, again showing the Shuttle to be a strong source of neutrons. Small spacecraft have relatively few locally produced neutrons as seen on Cosmos-2044 and also on the Orbiting Geophysical Observatory (OGO-6) satellite where only 3 to 4 percent corrections of the albedo neutron measurements resulted from neutrons produced locally in the spacecraft materials (Jenkins et al. 1971; see also Dudkin et al. 1992).

In earlier work, we had compared computational models with high linear energy transfer (LET) event rates that caused upsets on the Shuttle computers (Shinn et al. 1995), with CR-39 measurements on the Spacehab mission D1 (Shinn et al. 1995), with spectral measurements using a particle identification spectral telescope (Badhwar et al. 1995b), and with time-resolved lineal energy distributions in a tissue equivalent proportional counter (TEPC), (Shinn et al. 1998). In these studies, we found that the details of the vehicle geometry and materials, as well as the detector response, were required to be accurately modeled in order to relate the measured data to computed instrument responses based on computer evaluated flux at the detector location within the vehicle. Over-simplification of the details would usually result in poor comparisons. Through these comparisons, two weaknesses in the codes were identified: (i) lack of a description of meson production (Shinn et al. 1998) and (ii) lack of an adequate low energy neutron transport algorithm compatible with the HZETRN shielding code (Wilson et al. 1995; Clowdsley et al. 2000a,b). Most of these comparisons are determined by the charged particle environment except for the TEPC which is equally sensitive to neutrons and photons. Still there is great advantage, in terms of code testing, to evaluate the codes against measurements sensitive only (or primarily) to the neutron environment. In making such comparisons, we first need an improved description of the trapped proton environment and the albedo neutron environment, which make a non-negligible contribution to the total environment in LEO. In the present paper we will develop improved trapped radiation and albedo neutron environmental models, evaluate the total environment within the specific locations of the Shuttle and compare the findings with measured neutrons on specific Shuttle missions.

Models of the Natural Environment

Three sources of particles in the LEO environment are considered herein: galactic cosmic rays (GCR), particles trapped in the Earth's magnetic field, and neutrons produced as secondaries during interaction of the GCR with the Earth's atmosphere. The "splash,, electrons and protons are secondary particles produced in the atmosphere and are of energy too low to escape the geomagnetic field. These "splash,, particles follow the geomagnetic field lines to the mirror point where they reenter the atmosphere. They are of low intensity and are not treated herein. The particles are all modulated by the solar cycle (as represented by sunspot number, SSN) through various mechanisms, and near term ISS missions will be near solar maximum, as shown in figure 1.

Galactic Cosmic Rays

The GCR are represented by the environments evaluated by Badhwar and O'Neill (1995) for successive solar minima and maxima and interpolated herein according to the Deep River Neutron Monitor (DRNM), (Wilson et al. 1999). The variation of the DRNM over the present solar cycle with future projections is shown in figure 2. DRNM variations in future years are extrapolated according to correlation with the projected SNN already defined in figure 1. The Badhwar/O'Neill model is interpolated according to the smoothed sunspot numbers and at successive maxima and minima of the DRNM correlation functions (Wilson et al. 1999). The Smart and Shea (1983) vertical cutoff rigidities (scaled in altitude) are used to calculate the orbit-averaged geomagnetic transmission factors, including the effects of the Earth's shadow. The ISS GCR environment near the present solar maximum is shown in figure 3 outside the geomagnetic field and within the geomagnetic field in figure 4 during geomagnetic quiet times.

Trapped Radiations

The trapped radiations consist of two populations. The inner zone particles result from the decay of atmospheric neutrons as they leak from the Earth's atmosphere into the trapping region. The inner zone particles are lost from the trapping region by interaction with the tenuous atmosphere and generally have

long trapping lifetimes. The inner zone consists of both proton and electron decay products. The outer zone consists of electrons which are not really trapped but are continuously injected into the magnetospheric tail region and radially diffuse to lower altitudes until they are lost in the atmosphere near the polar regions. These outer zone electrons form the well-known aurora during geomagnetic disturbances. The average kinetic energy of either the outer or inner zone electrons is a few hundred keV, and these electrons are easily removed by the slightest amount of shielding and are mainly of concern to an astronaut in a space suit. Within any pressure vessel such as the Shuttle or ISS, the electrons are easily eliminated by the meteoroid bumper and pressure vessel. Only the protons with energies near or above the hundred MeV range are of concern within the Shuttle or ISS.

The particles trapped in the geomagnetic field were modeled from data obtained during two epochs of solar cycle 20 (the solar minimum of 1964 and the solar maximum of 1970), and best estimates of magnetic field coordinates were taken from current field models at the time of measurement (Atwell et al. 1989). The 1964 analysis using the magnetic field model IGRF-65/epoch 1964 resulted in particle population maps AP8 MIN and AE8 MIN for trapped protons and electrons, respectively. The 1970 analysis using the magnetic field model United States Coast and Geodetic Survey (US C&GS)/epoch 1970 resulted in the particle population maps of AP8 MAX and AE8 MAX. It was believed at one time that better estimates of particle environments could be gained by evaluating the population maps defined on invariant McIlwain coordinates using current magnetic field conditions. This interpolation would, for example, contain the westward shift of the South Atlantic anomaly observed in recent years by Badhwar et al. (1996). However, it was recognized by the Shuttle dosimetry group (Atwell et al. 1989) that large errors resulted from such a procedure, and we concluded that the use of the particle population maps, interpolated over the field model for which the population map was derived, would provide the best estimates of the long-term orbital averaged particle environments, even though the westward shift is not represented. A comparison of the Shuttle dosimetric results at various times in the last few solar cycles and the model calculations are shown in figure 5. The upper curve is for solar minimum (1964) and the lower curve for solar maximum (1970). The squares are interpolations that use the solar 10.7 cm radio output evaluated by Atwell et al. (1989).

Following the work of Atwell et al. (1989), we have used the 10.7 cm radio output ($F_{10.7}$, W/m^2) to scale the trapped electron environments as a function of solar cycle. The rationale is that the outer zone electrons are trapped through the magnetospheric tail and are lost after radial diffusion into the atmosphere near the polar regions. The injection and the atmospheric loss are correlated with the radio output at 10.7 cm, which is used herein as the appropriate interpolating function. The electron flux is assumed to be of the form

$$f_e(E) = f_{e,\min}(E)\, \exp(-\alpha_e F_{10.7}) \tag{1}$$

where $f_{e,\min}(E)$ is the electron flux at solar minimum and α_e is evaluated using AE8 MAX data derived from cycle 20 measurements (Wilson et al. 1999). In the model we use the prior 15-month average of the 10.7-cm radio output for $F_{10.7}$.

The proton environment has as its source the neutron albedo, and the losses occur through atmospheric interaction. The proton environment is then proportional, in steady state, to the source and the lifetime due to atmospheric interaction (Blanchard and Hess 1964). The interpolation procedure assumes a steady state solution to the population kinetic equations as the product of the albedo neutron source and the

lifetimes. This product is proportional to the product of the neutron monitor count rate and solar radio output at the 10.7 cm. The proton flux is then extrapolated by using the following functional form:

$$f_p(E) = f_{p,\min}(E) \exp[-\alpha_p (\mathrm{DRNM} \times F_{10.7})] \tag{2}$$

where $f_{p,\min}(E)$ is the proton flux at solar minimum, and α_p is evaluated by using the solar maximum $f_{p,\max}(E)$ derived from cycle 20 measurements, as will be described subsequently. In the model, the quantity (DRNM × $F_{10.7}$) is averaged over the prior 15 months. Following the recent analysis of Huston and Pfitzer (1998); (see also Huston, Kuck, and Pfitzer 1998), we use the proton flux at solar minimum with $f_{p,\min}(E) = 2.15 f_{\mathrm{AP8\ MIN}}(E)$ and at solar maximum with $f_{p,\max}(E) = 2.57 f_{\mathrm{AP8\ MAX}}(E)$.

The electron and proton environment near the current solar maximum for the ISS orbit of 51.6° inclination and an altitude of 400 km is shown in figures 6 to 9. Figure 6 shows the electron flux at three energy thresholds (0.5, 1, and 3 MeV) as a function of time. The curves are found by interpolation using a prior 15-month average of the radio flux data with assumed exponential dependence in equation (1). The relation of the flux in 2001 and the AE8 MIN and AE8MAX models is shown in figure 7. The proton flux is assumed to depend on the 15-month average of the Deep River Neutron Monitor count rate times the radio flux output, with exponential dependence as given by equation (2). The results are shown in figure 8 near the current solar maximum. The proton flux is shown for comparison with AP8 MIN and AP8 MAX in figure 9. A comparison with the NOAAPRO model (that model is limited to integral flux above 16, 30, and 80 MeV, respectively) is shown in figure 10.

Neutron Albedo

Albedo neutrons result from the interaction of cosmic rays with the Earth's atmosphere. As the cosmic ray intensities are modulated by the solar activity, so are the atmospheric neutrons modulated with time. The atmospheric neutron model is a parametric fit to data gathered by the Langley Research Center studies of the radiations at supersonic transport (SST) altitudes during the years 1965 to 1971 that cover the rise and decline of solar cycle 20. Scaling of the data with respect to geomagnetic cutoff, altitude, and modulation of the Deep River Neutron Monitor was found to allow mapping of the environment to all locations at all times, resulting in an empirically based model for atmospheric neutrons (Wilson et al. 1991). The basic data consisted of fast neutron spectrometer measurements encapsulated by a charged particle anticoincidence scintillator that used pulse shape discrimination to reject gamma rays (Korff et al. 1979). The model was based on global surveys with airplanes and balloons. The latitude surveys by balloons and aircraft are shown for the transition maximum and at subsonic aircraft altitudes of 250 g/cm^2 in figure 11. The curves in the figure are our approximation to the data and are given in terms of rigidity R (GV), atmospheric depth x (g/cm^2), and Deep River Neutron Monitor count rate C in percent of the maximum (7157) by

$$\phi(x,R,C) = f(R,C) \exp(-x/\lambda) - F(R,C) \exp(-x/\Lambda) \tag{3}$$

where

$$f(R,C) = \exp(250/\lambda)\, \phi_G(R,C) \tag{4}$$

$$F(R,C) = (\Lambda/\lambda) f(R,C) \exp(x_m/\Lambda - x_m/\lambda) \tag{5}$$

and

$$\Lambda = \lambda[1 - \phi_m(R,C)\ \exp(x_m/\lambda)/f(R,C)] \tag{6}$$

$$x_m = 50 + \ln\{2000 + \exp[-2(C - 100)]\} \tag{7}$$

$$\begin{aligned}\phi_\sigma(R,C) = {} & 0.17 + [0.787 + 0.035\ (C - 100)]\ \exp(-R^2/25) \\ & + \{-0.107 - 0.0265\ (C - 100) \\ & + 0.612\ \exp[(C - 100)/3.73]\}\ \exp(-R^2/139.2)\end{aligned} \tag{8}$$

$$\begin{aligned}\phi_m(R,C) = {} & 0.23 + [1.1 + 0.0167\ (C - 100)]\ \exp(-R^2/81) \\ & + \{0.991 + 0.051\ (C - 100) \\ & + 0.4\ \exp[(C - 100)/3.73]\}\ \exp(-R^2/12.96)\end{aligned} \tag{9}$$

$$\lambda = 160 + 2\ R \tag{10}$$

where λ is the neutron attenuation length deep in the atmosphere and is slightly dependent on the energies of the incoming particles as determined by R.

The neutron environmental model is shown in figure 11 in comparison to experimental measurements of the Korff group (Korff et al. 1979). The model in the above equations (shown in fig. 11) is based on measurements within the atmosphere and often at SST and commercial aircraft altitudes. The albedo consists of those neutrons leaking from the top of the atmosphere (over 50 km) into space. The albedo is closely related to the neutrons at 48 g/cm^2 depth in the atmosphere, which is the upper range of validity of the atmospheric model of equations (3) to (10).

The 1–10 MeV flux, given by equations (3) to (10) at the depth x of 48 g/cm^2, describes the dependence on solar cycle, latitude, and longitude. The leakage flux $F_L(E)$ is closely related to the differential flux $\phi(E,\mathbf{\Omega})$ at the top of the atmosphere as follows:

$$F_L(E) = \int \cos\theta\ \phi(E,\mathbf{\Omega})\ d\mathbf{\Omega} \tag{11}$$

where $\cos\theta$ is the direction cosine of the velocity vector with the zenith. There are unresolved differences among various measurements of the leakage flux, which is in part the assumed angular dependence of the differential flux. The ratio of leakage flux to flux is given by the New York University (NYU) group (Korff et al. 1979) in table 1, which we use in the present model. The leakage flux was measured on the OGO-6 satellite by the University of New Hampshire (Lockwood 1972) during June 1969. The leakage flux spectrum was measured (Jenkins et al. 1971; Preszler et al. 1972) and calculated (Korff et al. 1979) by various groups over Palestine, Texas during September 1971, as shown in figure 12. The curve shown in figure 12 for the leakage is

$$F_L(E) = \begin{cases} 0.065/E & \text{for } E \le 10\ \text{MeV} \\ 0.0026\ \exp(-0.011E) & \text{for } E > 10\ \text{MeV} \end{cases} \tag{12}$$

The dashed curve in figure 12 is the corresponding angular integral of the differential flux. We have used these data, the leakage-to-flux ratio, and the atmospheric neutron model to extrapolate the 1–10 MeV

neutron flux to all times and locations at the top of the atmosphere. The total leakage flux is shown in figure 13 at various solar maxima and minima, and in particular, with the measurements on the OGO-6 satellite during June 1969, which was a local maximum of cycle 20 (i.e., local minimum of the DRNM). The leakage flux at the top of the atmosphere is extrapolated to low Earth orbit altitude according to Gauss's law (varies as r^{-2}). There are some inconsistencies among various groups about specific neutron field related quantities. The present model is biased to the Palestine spectrum of September 1971, the OGO-6 latitude dependence during the local DRNM minimum of June 1969, and solar cycle dependence of the high altitude atmospheric neutron measurements, as is clear from the previous discussion.

Evaluation of the Induced Environment

The charged particle environment on the Shuttle has been experimentally studied in detail using track detectors, charged particle telescopes, and tissue equivalent proportional counters that provide a basis for evaluating our understanding of environmental models, transport procedures, and engineering model databases that represent the distribution of Shuttle materials about the measurement locations. Good success has been achieved in predicting the internal Shuttle charged particle environmental components (Badhwar et al. 1995b; Shinn et al. 1995, 1998). A weakness in those earlier comparisons was the lack of attention given to the neutron component. Neutron measurements were made by Keith et al. (1992) using a Bonner sphere setup on STS-31 and STS-36, which will be the focus of the present evaluation. One limitation of the measurements is the range of sizes in the Bonner sphere setup, which ranged from 2 to 8 in. The energy range is limited to below about 15 MeV neutron energies. Analysis of the measurements was made by fitting a simple power law for the flux spectrum (see "Old flux,, entries in table 2) and is used herein as a basis of comparison. For a reanalysis of the Bonner sphere data, see Badhwar et al. (2001), in which an approximate account of the higher energy neutrons above 15 MeV on the Bonner sphere activation rates was made. These results are given as the "New flux,, entries in table 2.

The models for the natural environment are discussed in the previous section, and the induced neutron environment is evaluated by using the HZETRN code with an improved neutron transport procedure and definition of the vehicle geometry. The types and energy distributions of particles transmitted through a shield material require the solution to a transport description of the process with appropriate boundary conditions that are related to the external space radiation environment. The relevant transport equations are the linear Boltzmann equations derived on the basis of conservation principles for the flux density $\phi_j(\boldsymbol{x},\boldsymbol{\Omega},E)$ of type j particles at location x moving in direction $\boldsymbol{\Omega}$ with energy E as

$$\boldsymbol{\Omega}\bullet\nabla\phi_j(\boldsymbol{x},\boldsymbol{\Omega},E) = \sum\int \sigma_{jk}(\boldsymbol{\Omega},\boldsymbol{\Omega}',E,E')\,\phi_k(\boldsymbol{x},\boldsymbol{\Omega}',E')\,d\boldsymbol{\Omega}'\,dE' - \sigma_j(E)\,\phi_j(\boldsymbol{x},\boldsymbol{\Omega},E) \tag{13}$$

where $\sigma_j(E)$, $\sigma_{jk}(\boldsymbol{\Omega},\boldsymbol{\Omega}',E,E')$ are the media macroscopic cross sections for various atomic and nuclear processes, including spontaneous disintegration. Equation (13) is to be solved subject to the boundary condition

$$\phi_j(\boldsymbol{\Gamma},\boldsymbol{\Omega},E) = \Psi_j(\boldsymbol{\Omega},E) \quad \text{where } \boldsymbol{n}\cdot\boldsymbol{\Omega} < 0 \tag{14}$$

where $\boldsymbol{\Gamma}$ denotes a point on the boundary, $\boldsymbol{n}$ is the outward directed unit normal at $\boldsymbol{\Gamma}$, and $\Psi_j(\boldsymbol{\Omega},E)$ is the external fluence (space environment). In general, there are hundreds of particle fields $\phi_j(\boldsymbol{x},\boldsymbol{\Omega},E)$ with several thousand cross-coupling terms $\sigma_{jk}(\boldsymbol{\Omega},\boldsymbol{\Omega}',E,E')$ through the integral operator in equation (13). The total cross section $\sigma_j(E)$ with the medium for each particle type of energy E may be expanded as

$$\sigma_j(E) = \sigma_{j,at}(E) + \sigma_{j,el}(E) + \sigma_{j,r}(E) \tag{15}$$

where the first term refers to collision with atomic electrons, the second term is for elastic nuclear scattering, and the third term describes nuclear reactive processes and is ordered as $1 : 10^{-5} : 10^{-8}$. This ordering allows flexibility in expanding solutions to the Boltzmann equation as a sequence of physical perturbative approximations. Special problems arise in the perturbation approach for neutrons for which the nuclear elastic process appears as the first-order perturbation and has been the focus of recent research as described next. The double differential particle production and fragmentation cross sections $\sigma_{jk}(\mathbf{\Omega},\mathbf{\Omega}',E,E')$ of equation (13) are separated into an isotropic contribution and a remainder as

$$\sigma = \sigma_F + \sigma_{\text{iso}} \tag{16}$$

where the remainder σ_F consists of only forward directed secondary particles and σ_{iso} is dominated by lower energy particles produced in the reaction, creating a forward propagating component and a diffuse component.

The solution to equation (13) can likewise be separated into two parts, for which σ_F appears only in an equation like equation (13), with solution ϕ_F and a second equation for the diffuse components in which σ_{iso} appears in equation (13) but with source terms from coupling to the ϕ_F field through σ_{iso}. The solution to equation (13) for ϕ_F can be written in operational form as

$$\phi_F = G_F \Psi_B \tag{17}$$

where Ψ_B is the inbound flux at the boundary, and G_F is the Green's function associated with σ_F, which reduces to a unit operator on the boundary. We will evaluate equation (17) by using the marching procedure of the HZETRN code. There remains the evaluation of the remainder terms σ_{iso} of equation (13), especially the low-energy neutron transport.

The remainder of equation (13) following the separation given by equation (16) is

$$\mathbf{\Omega}\bullet\nabla\phi_j(\boldsymbol{x},\mathbf{\Omega},E) = \sum\int \sigma_{\text{iso},jk}(E,E')\,\phi_k(\boldsymbol{x},\mathbf{\Omega}',E')\,d\mathbf{\Omega}'\,dE' - \sigma_j(E)\,\phi_j(\boldsymbol{x},\mathbf{\Omega},E) + g_j(E,\boldsymbol{x}) \tag{18}$$

where the source term $g_j(E,\boldsymbol{x})$ results from the collisional σ_{iso} source with the σ_F field. The charged particle fields of equation (18) can be solved analytically, leaving the low-energy neutron fields to be evaluated by using energy multigroup methods and approximating the integral term by the mean value theorem evaluated at a parametric energy point. It requires a solution to a boundary value problem for the distribution of neutron sources along a 512 array of directions about each location within the vehicle where the fields are to be evaluated. This procedure can be time consuming (a few minutes per ray per evaluation point) on a serial machine when one is mapping the radiation environment at many locations within the human body and at many locations within a complex structure such as the Shuttle, RLV, ISS, or Mars mission vehicles and habitats. The solution methodology implies a great deal of repeated operations (for each direction) with differences only in the distribution of source terms, distances to the boundaries, and boundary conditions. This high degree of parallelism will be used to greatly speed the computation by doing all 512 directions in parallel. Other parallel operations could also be used in the solution of the ϕ_F fields that are solved by marching procedures which require modifications of the HZETRN code configuration.

The induced neutrons are represented by a forward component wherein the usual HZETRN transport procedure (Wilson et al. 1995) is used and a diffuse component, in which multidirectionality of the neutrons is accounted for (Clowdsley et al. 2000b).

Results for STS-31 and STS-36

The flight dates and orbital parameters of STS-31 and STS-36 are given in table 2. STS-36 is shown as a low-altitude, high-inclination flight dominated by the GCR in the first quarter of 1990. The STS-31 flight was a high-altitude, low-inclination flight dominated by the trapped proton environment a few months later. Both flights occurred near the maximum modulation effects of the solar cycle. The GCR, trapped particles, and neutron albedo were evaluated by using the above described models and were transported into the Shuttle materials by using the multigroup-neutron/HZETRN code (Clowdsley et al. 2000a,b).

The results for the STS-36 flight are shown in figure 14. The two JSC analyses are shown as the dot-dash (old) and dash curves extending downward from the upper left corner of the graph and terminating at 15 MeV. At this low altitude and high inclination mission, most of the induced neutrons are from the GCR and neutron albedo. The neutrons induced by the natural environment are shown in the figure as the solid curve. The results for the STS-31 flight are shown in figure 15. The JSC data are shown as the dot-dash (old) and dash (new) lines extending downward from the upper left corner. In this low-inclination high-altitude mission, the neutrons induced by the trapped protons in the Shuttle materials are the dominant neutron component. The GCR contribute neutrons at much higher energies but contribute little in the range of the measurements. The spectral shape in the important 1–10 MeV region from the neutrons, induced by the trapped radiations and by the GCR, is quite distinct. It is not clear whether this peculiar shape is a limitation of the current preliminary nuclear database for developing solution methods (Wilson et al. 1991) or a fundamental difference in the production processes. Also, it is not clear whether the spectral differences with the JSC measurements are a result of the simplified analysis of the Bonner sphere data used in reducing the measurements. An improved database for ISS is currently under development and is expected to shed more light on these issues.

It is of interest to evaluate the importance of the neutron environment on astronaut exposures during Shuttle operations in LEO. The neutron measurements were taken at dosimeter location 2 (DLOC2) within the Shuttle vehicle. It is here we evaluate the exposure of the astronaut by using the computerized anatomical man (CAM) model for skin, ocular lens, and blood forming organ (BFO). The results for the STS-36 flight at low altitude and high inclination where the GCR and neutron albedo dominate the exposure are given in table 3. It is seen from the table that neutrons from the albedo and those induced in the Shuttle materials contribute from 11 to 15 percent of the exposure to critical organs. In this case, the Shuttle environment is dominated by the GCR and the neutrons are predominantly induced through interactions with the Shuttle materials. Similar results are shown in table 4 for the high altitude and low inclination orbit of STS-31. In this case, the Shuttle is effectively shielded by the geomagnetic field, and the exposures are dominated by the trapped radiations.

Long-Term Variations

As a test on variation over long time periods, we compare the calculated dose with the log of Shuttle data over many years (1983 to 2000), recently published by Badhwar (1999, 2002). We have only evaluated a sampling of the reported data at four locations in the Shuttle (DLOC1-4) with results given in table 5. It is difficult to judge any systematic time behavior as the measurements were over a broad range of altitudes and inclinations. The lower inclinations are dominated by trapped radiations at almost all altitudes and provide a rigid test on the trapped particle environment modulation. The 51.6° inclinations have comparable contributions from both trapped particles and galactic cosmic rays. The model results are generally lower than the measurements by ten percent or less. The exceptions are two low inclination

and high altitude flights (STS-31 and STS-82) which are 3.4 and 6.9 percent higher than the data, respectively.

Concluding Remarks

Three things have been accomplished in the present analysis. First, an improved description of the LEO environment has been developed in terms of time dependent trapped radiation models and an improved neutron albedo model. The second accomplishment is an improved computational procedure for evaluation of the induced neutron environment within spacecraft interiors. Finally, a step in validating the means by which we evaluate the mixed radiation environment by using environmental models, computational transport procedures, and vehicle geometry models has been made. Although the computational procedures for GCR components appear well represented by the JSC measurements, the trapped environment comparisons leave some open questions because the reduced spectrum from the measurements on the low-inclination flight of STS-31 appears less structured than the computational model. This difference may be due to the simplified analysis of the measured data or the uncertainty in the nuclear database.

References

Atwell, W.; Beever, E. R.; Hardy, A. C.; Richmond, R. G.; and Cash, B. L.: Space Radiation Shielding Analysis and Dosimetry for the Space Shuttle Program. In *High-Energy Radiation Background in Space*, A. C. Rester and J. I. Trombka, eds., AIP Conference Proceedings 186, New York, 1989, pp. 289–296.

Badhwar, G. D.; Cucinotta, F. A.; Braby, L. A.; and Konradi, A.: Measurements on the shuttle of the LET spectra of galactic cosmic radiation and comparison with the radiation transport model. *Radiat. Res.*, vol. 139, 1994, pp. 344–351.

Badhwar, G. D.; Atwell, W.; Benton, E. V.; Frank, A. L.; Keegan, R. P.; Dudkin, V. E.; Karpov, O. N.; Potapov, Yu. V.; Akopova, A. B.; Magradze, N. V.; Melkumyan, L. V.; and Rshtuni, Sh. B.: A study of the radiation environment onboard the space shuttle flight STS-57. *Radiat. Meas.*, vol. 24, 1995a, pp. 283–289.

Badhwar, G. D.; Patel, J. U.; Cucinotta, F. A.; and Wilson, J. W.: Measurements of secondary particle energy spectrum in the space shuttle. *Radiat. Meas.*, vol. 24, 1995b, pp. 129–138.

Badhwar, G. D. and O'Neill, P. M.: An improved model of galactic cosmic radiation for space exploration missions. *Nucl. Tracks Radiat. Meas.*, vol. 20, 1995, pp. 410–427.

Badhwar, G. D.; Golightly, M. J.; Konradi, A.; Atwell, W.; Kern, J. W.; Cash, B.; Benton, E. V.; Frank, A. L.; Sanner, D.; Keegan, R. P.; Frigo, L. A.; Petrov, V. M.; Tchernykh, I. N.; Akatov, Yu. A.; Shurshakov, V. A.; Arkhangelsky, V. V.; Kushin, V. V.; Klyachin, N. A.; Vana, N.; and Schoner, W.: In-flight radiation measurements on STS-60. *Radiat. Meas.*, vol. 26, 1996, pp. 17–34.

Badhwar, G. D.: Radiation dose rates in space shuttle as a function of atmospheric density. *Radiat. Meas.*, vol. 30, 1999, pp. 401–414.

Badhwar, G. D.; Keith, J. E., and Cleghorn, T. F.: Neutron measurements onboard the space shuttle. *Radiat. Meas.*, vol. 33, 2001, pp. 235–241.

Badhwar, G. D.: Shuttle radiation dose measurements in international space station orbits. *Radiat. Res.*, vol. 157, 2002, pp. 69–75.

Blanchard R. C.; and Hess, W. N.: Solar cycle changes in inner zone protons. *J. Geophys. Res.*, vol. 69, 1964, p. 3927.

Clowdsley, M. S.; Heinbockel, J. H.; Kaneko, H.; Wilson, J. W.; Singleterry, R. C.; and Shinn, J. L.: A comparison of the multigroup and collocation methods for solving the low-energy neutron Boltzmann equation. *Can. J. Phys.*, vol. 78, 2000a, pp. 45–56.

Clowdsley, M. S.; Wilson, J. W.; Heinbockel, J. H.; Tripathi, R. K.; Singleterry, R. C.; and Shinn, J. L.: *An Improved Elastic and Nonelastic Neutron Transport Algorithm for Space Radiation.* NASA TP-210299, 2000b.

Dudkin, V. E.; Potapov, Yu. V.; Akopova, A. B.; Melkumyan, L. V.; Rshtuni, Sh. B.; Benton, E. V.; and Frank, A. L.: Neutron fluences and energy spectra in the Cosmos-2044 Biosatellite orbit. *Nucl. Tracks Radiat. Meas.*, vol. 20, 1992, pp. 139–141.

Dudkin, V. E.; Karpov, O. N.; Potapov, Yu. V.; Akopova, A. B.; Magradze, N. V.; Moiseenko, A. A.; Melkumyan, L. V.; and Rshtuni, Sh. B.: Studying radiation environment onboard STS-55 and STS-57 by the method of passive detectors. *Radiat. Meas.*, vol. 25, 1995, pp. 483–484.

Huston, S. L.; Kuck, G. A.; and Pfitzer, K. A.: Solar cycle variation of the low-altitude trapped proton flux. *Adv. Space Res.*, vol. 21(12), 1998, pp. 1625–1634.

Huston, S. L., and Pfitzer, K. A.: *Space Environment Effects: Low-Altitude Trapped Radiation Model.* NASA CR-208593, 1998.

Jenkins, R. W.; Ifedili, S. O.; Lockwood, J. A.; and Razdan, H.: The energy dependence of the cosmic-ray neutron leakage flux in the range 0.01–10 MeV. *J. Geophys. Res.*, vol. 76, 1971, pp. 7470–7478.

Keith, J. E.; Badhwar, G. D.; and Lindstrom, D. J.: Neutron spectrum and dose-equivalent in shuttle flights during solar maximum. *Nucl. Tracks Radiat. Meas.*, vol. 20, 1992, pp. 41–47.

Korff, S. A.; Mendell, R. B.; Merker, M.; Light, E. S.; Verschell, H. J.; and Sandie, W. S.: *Atmospheric Neutrons.* NASA CR-3126, 1979.

Lobakov, A. P.; Lyagushin, V. I.; Panasyuk, M. I.; Petrov, V. M.; and Shavrin, P. I.: Long-term measurements of the neutron flux aboard the "Mir„-type space station. *Nucl. Tracks Radiat. Meas.*, vol. 20, 1992, pp. 55–58.

Lockwood, J. A.: Neutron measurements in space. *Space Sci. Rev.*, vol. 14, 1972, pp. 663–719.

Preszler, A. M.; Simnett, G. M.; and White, R. S.: Earth albedo neutrons from 10–100 MeV. *Phys. Rev. Letters*, vol. 28, 1972, pp. 982–984.

Shinn, J. L.; Cucinotta, F. A.; Wilson, J. W.; Badhwar, G. D.; O'Neill, P. M.; and Badavi, F. F.: Effects of target fragmentation on evaluation of LET spectra from space radiations in low Earth orbit (LEO) environment—Impact on SEU predictions. *IEEE Trans. Nucl. Sci.*, vol. 42, 1995, pp. 2017–2025.

Shinn, J. L.; Cucinotta, F. A.; Simonsen, L. C.; Wilson, J. W.; Badavi, F. F.; Badhwar, G. D.; Miller, J.; Zeitlin, C.; Heilbronn, L.; Tripathi, R. K.; Clowdsley, M. S.; Heinbockel, J. H.; and Zapsos, M. A.: Validation of a comprehensive space radiation transport code. *IEEE Trans. Nucl. Sci.*, vol. 45, 1998, pp. 2711–2719.

Smart, D. F.; and Shea, M. A.: Geomagnetic transmission functions for 400 km altitude satellite. *18th International Cosmic Ray Conference—Conference Papers* MG Sessions, vol. 3, Tata Inst. of Fundamental Research (Colaba, Bombay), 1983, pp. 419–422.

Wilson, J. W.; Townsend, L. W.; and Farhat, H.: Cosmic-ray neutron albedo dose in low-Earth orbits. *Health Phys.*, vol. 57, 1989, pp. 665–668.

Wilson, J. W.; Townsend, L. W.; Schimmerling, W. S.; Khandelwal, G. S.; Khan, F.; Nealy, J. E.; Cucinotta, F. A.; Simonsen, L. C.; Shinn, J. L.; and Norbury, J. W.: *Transport Methods and Interactions for Space Radiations.* NASA RP-1257, 1991.

Wilson, J. W.; Badavi, F. F.; Cucinotta, F. A.; Shinn, J. L.; Badhwar, G. D.; Silberberg, R.; Tsao, C. H.; Townsend, L. W.; and Tripathi, R. K.: *HZETRN: Description of a free-space ion and nucleon transport and shielding computer program.* NASA TP-3495, 1995.

Wilson, J. W.; Kim, M.-H.; Cucinotta, F. A.; Badavi, F. F.; Shinn, J. L.; Tai, H.; Badhwar, G. D.; and Atwell, W.: *Solar Cycle Variation and Application to the Space Radiation Environment.* NASA TP-209369, 1999.

Wu, H.; Atwell, W.; Cucinotta, F. A.; and Yang, C. Estimate of Space Radiation-Induced Cancer Risks for International Space Station Orbits. NASA TM-104818, 1996.

Table 1. Ratio of Leakage Flux to Flux as Function of Energy and Geomagnetic Cutoff

	Leakage to flux ratio for energy (MeV) of —					
P_c, GV	<0.001	0.001–1	1–10	10–19	19–100	100–2000
0	0.07	0.63	0.55	0.48	0.45	0.38–0.23
17	0.07	0.64	0.56	0.49	0.53	0.46–0.39

Table 2. Space Shuttle Measurements of LEO Environment

Parameter	STS-36	STS-31
Launch date	28 Feb. 90	24 Apr. 90
Duration (days)	4.43	5.05
Altitude (km)	246	617
Inclination (°)	62	28.5
Old flux (n/cm^2 MeV min)	$5.92(\pm 0.27)/E^{0.765}$	$45.1(\pm 1.9)/E^{0.765}$
New flux (n/cm^2 MeV min)		
Eth < E < 20 MeV	$0.82E^{-1} + 8.5e^{-E/4.74}$	$6.78E^{-1} + 59e^{-E/4.74}$
20 < E < 100 MeV	$0.82E^{-1} + 300E^{-2.6}$	$6.78E^{-1} + 2090E^{-2.6}$
100 < E < 400 MeV	$0.022e^{-E/100} + 300E^{-2.6}$	$0.185e^{-E/100} + 2090E^{-2.6}$
TLD Dose, μGy/d	89	1660

Table 3. Exposure of Critical Organs Within the Shuttle During STS-36 at DLOC2

STS-36 at 62° inclination and 246-km altitude during February 1990. Values in parentheses are for the charged particle components only.		
GCR daily exposure	Dose, μGy/d	Dose equivalent, μSv/d
Skin	55.6(53.4)	219.5(205.1)
Ocular lens	54.6(51.9)	213.9(195.1)
BFO	54.3(50.9)	184.1(167.3)
Trapped and albedo daily exposure	Dose, μGy/d	Dose equivalent, μSv/d
Skin	0.64(0.32)	3.1(0.89)
Ocular lens	0.65(0.27)	3.1(0.39)
BFO	0.59(0.12)	2.4(0.17)

Table 4. Exposure of Critical Organs Within the Shuttle During STS-31 at DLOC2

STS-31 at 28.5° inclination and 617-km altitude during April 1990. Values in parentheses are for the charged particle components only.		
GCR daily exposure	Dose, μGy/d	Dose equivalent, μSv/d
Skin	-	-
Ocular lens	-	-
BFO	-	-
Trapped and albedo daily exposure	Dose, μGy/d	Dose equivalent, μSv/d
Skin	2540(2540)	3830(3750)
Ocular lens	2520(2510)	3560(3470)
BFO	1610(1600)	2300(2230)

Table 5. Comparison of Present Model With Shuttle Flight Data

Flight	Date	Collected data, μGy/d			Calc., μGy/d
		DRNM*	DLOC	TLD†	
STS-41A	11/83	6421	3	64.6	59.6
STS-51D	4/85	6661	4	917.4	889.3
STS-31	4/90	5701	1	2141	2290
STS-43	8/91	5894	4	20.7	18.6
STS-62	3/94	6771	1	94.3	89.2
STS-65	7/94	6822	2	28.3	25.1
STS-67	3/95	6925	3	250.8	238.1
STS-80	11/96	6973	4	264.4	256.5
STS-82	2/97	7074	1	2978	3080
STS-91	6/98	6894	1	89.1	83.2
STS-101	5/00	6460	2	140.8	131.1
STS-92	10/00	6417	2	165.9	153.4

*Deep River Neutron Monitor count rate.

†GCR corrected TLD-100 data.

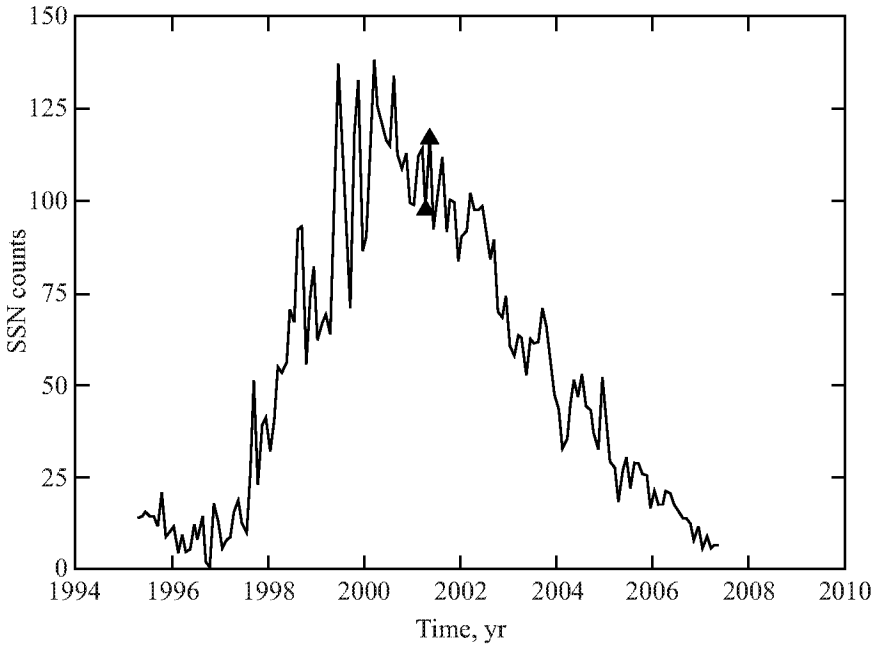

Figure 1. Sunspot number (SNN) for International Space Station (ISS) environment in first week of June 2001 according to present model; 400 km × 51.6°.

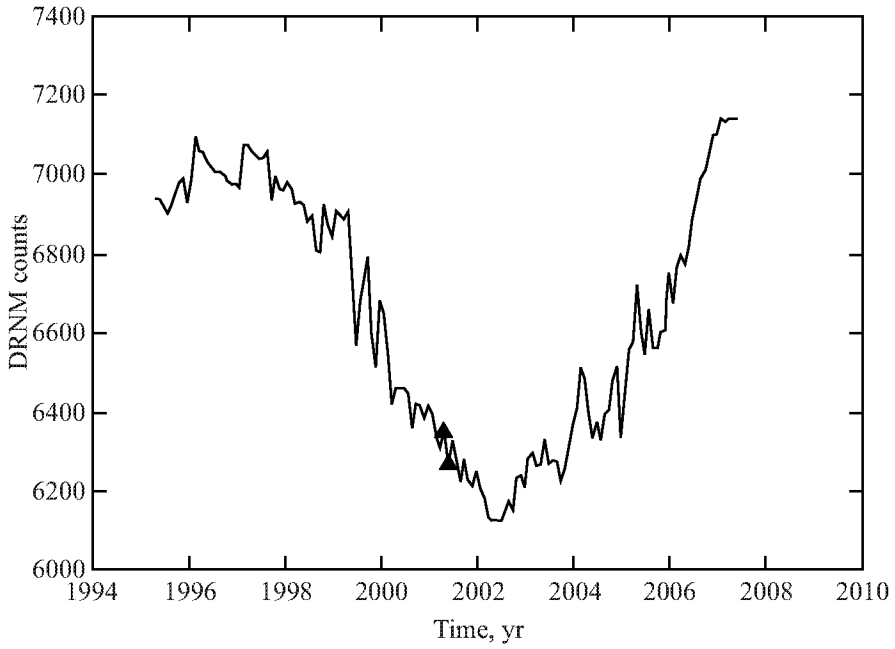

Figure 2. Deep River Neutron Monitor (DRNM) count rate for ISS environment in first week of June 2001 according to present model; 400 km × 51.6°.

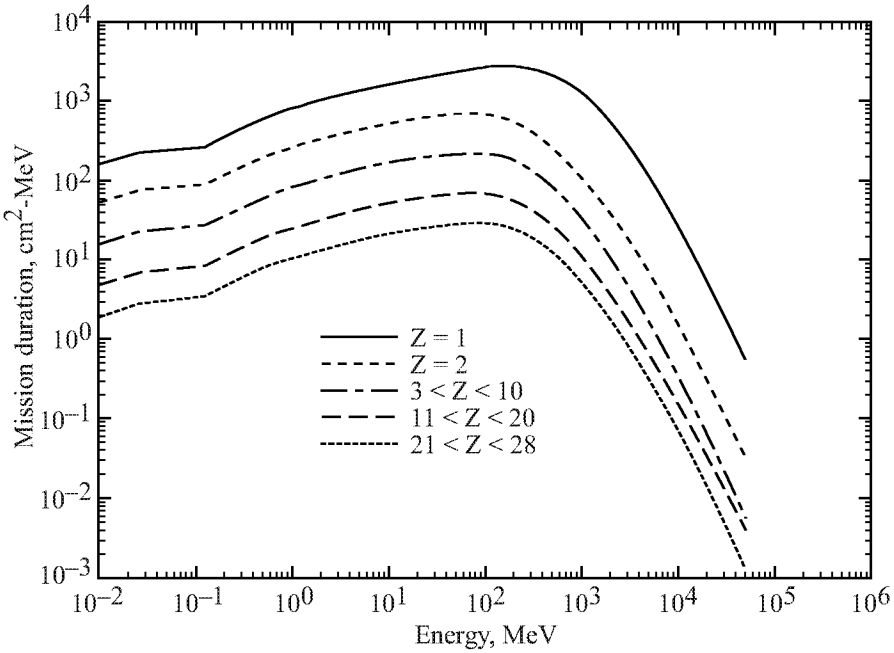

Figure 3. Galactic cosmic ray (GCR) environment for first week of June 2001 outside the geomagnetic field; ISS GCR free space, 400 km × 51.6°.

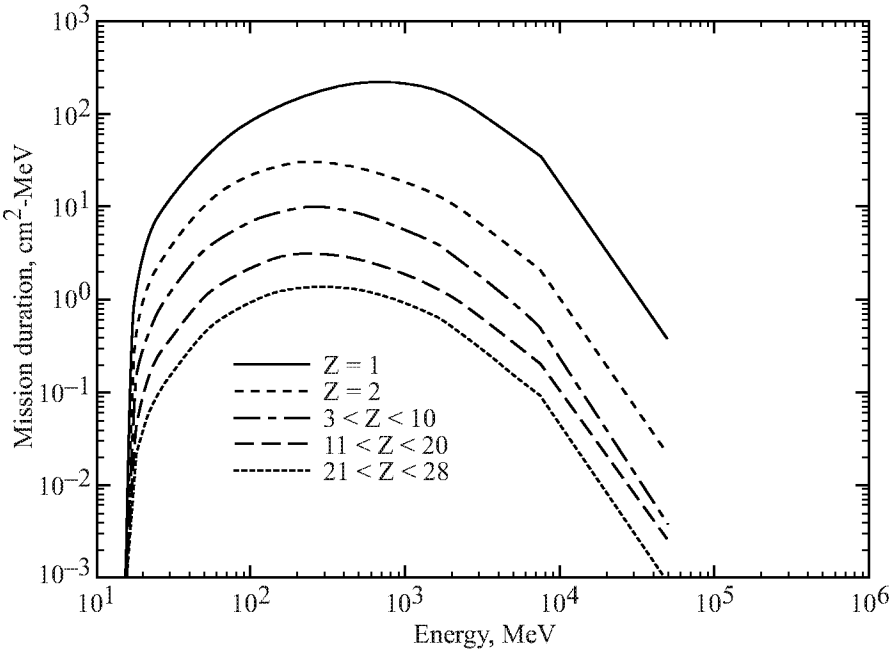

Figure 4. ISS GCR environment in first week of June 2001 according to the present model; ISS GCR + cutoff field; 400 km × 51.6°.

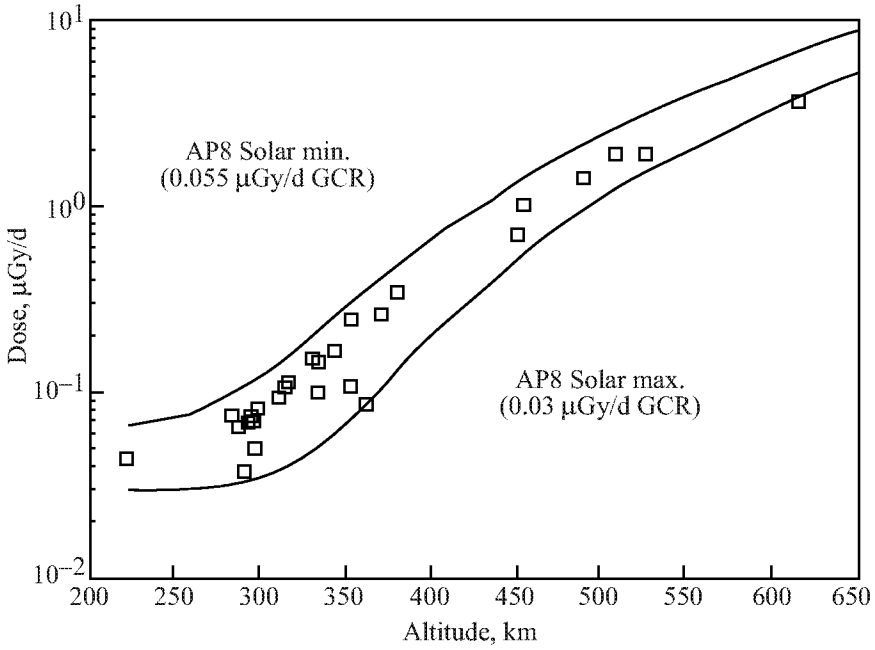

Figure 5. Shuttle measurements in low inclination, low Earth orbit (LEO) compared to model calculations (Atwell et al. 1989).

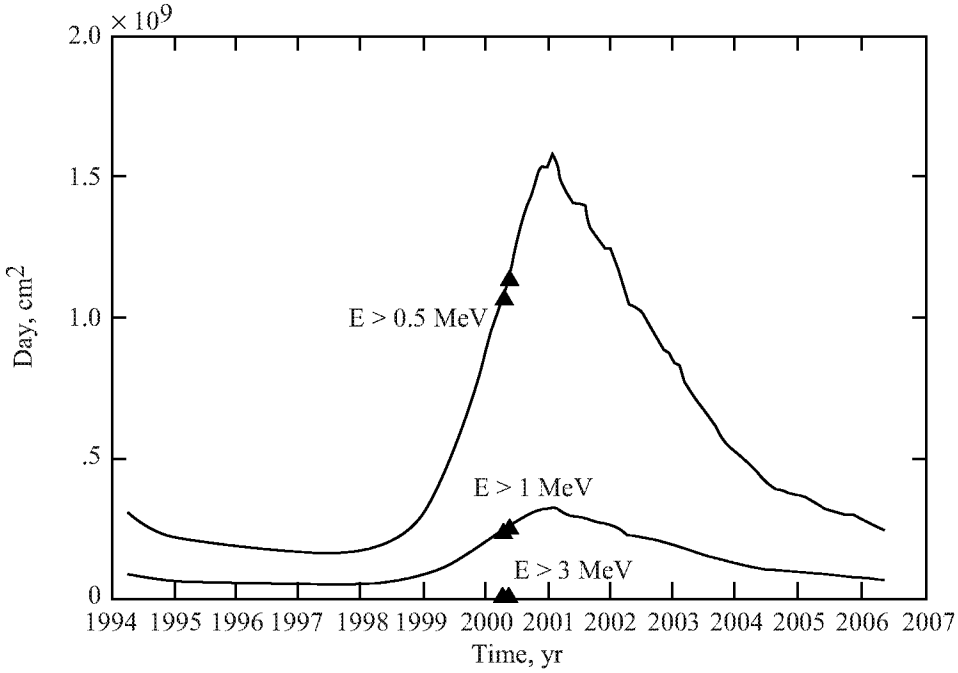

Figure 6. ISS electron environment for first week of June 2001. ISS trapped electron field; 400 km × 51.6°.

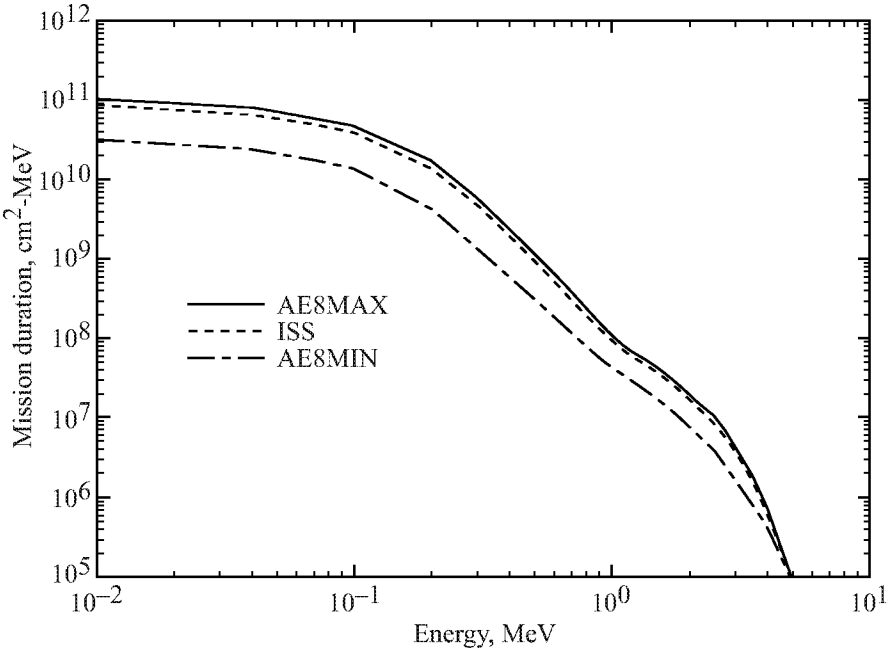

Figure 7. ISS electron differential spectrum for first week of June 2001; 400 km × 51.6°.

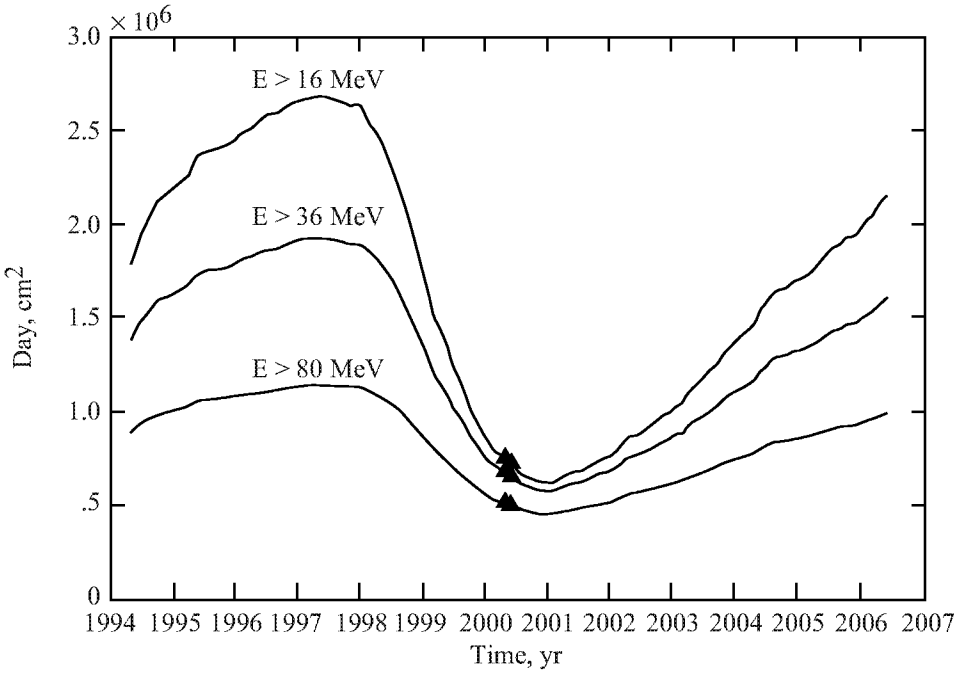

Figure 8. ISS proton environment for first week of June 2001; ISS trapped proton field, 400 km × 51.6°.

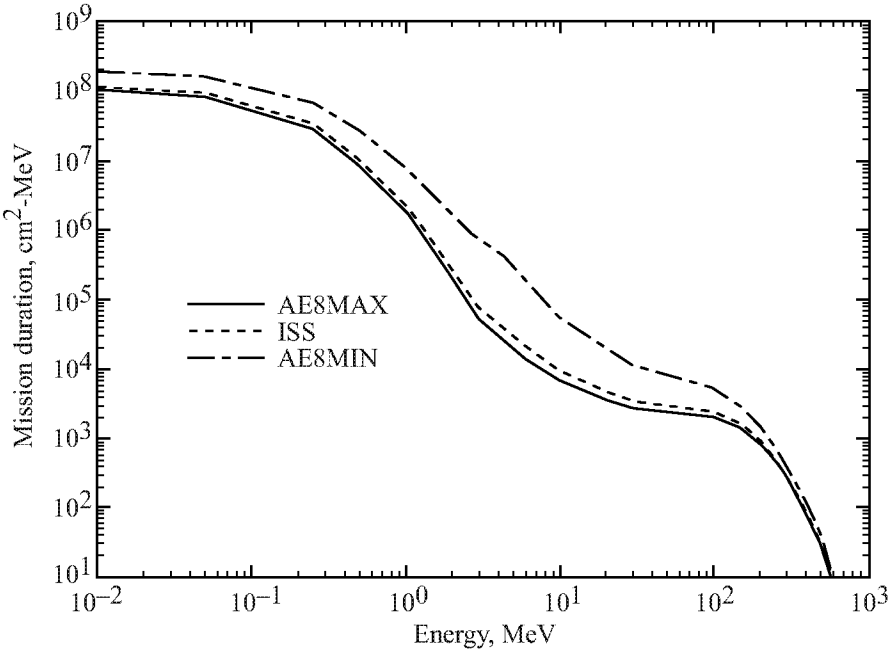

Figure 9. ISS proton differential spectrum for first week of June 2001; ISS trapped proton field, 400 km × 51.6°.

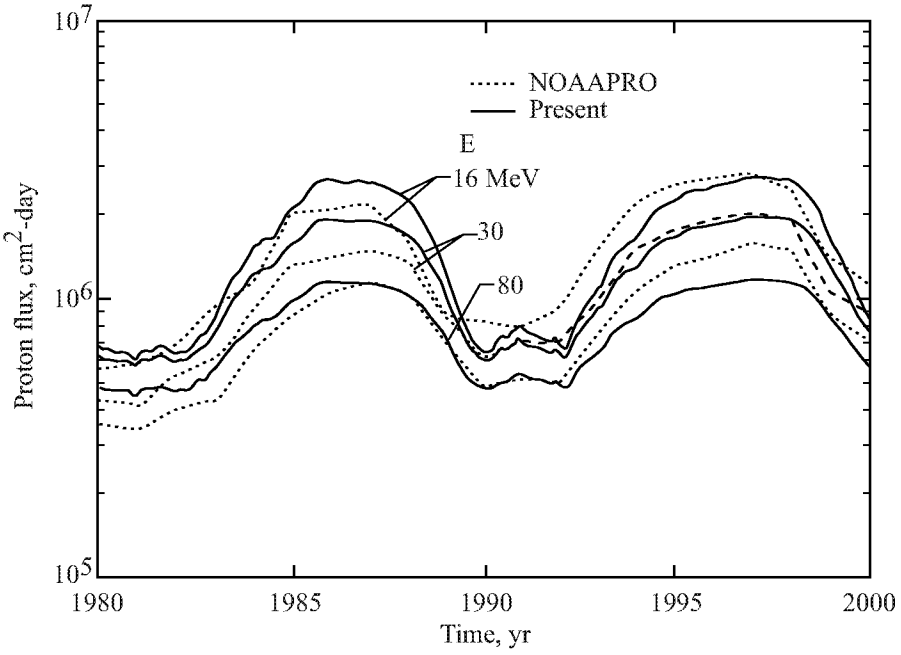

Figure 10. Predicted proton flux levels of the present model and those of the NOAAPRO model.

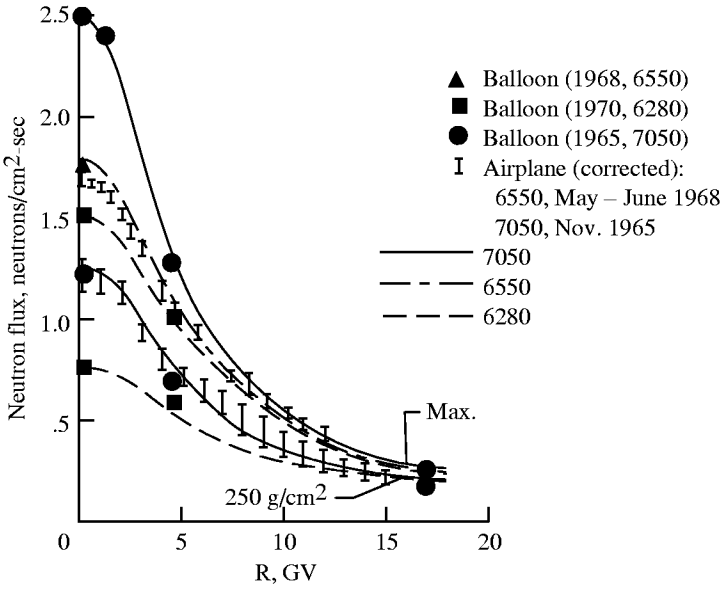

Figure 11. Fast neutron flux (in the range from 1 to 10 MeV) at the transition maximum and 250 g/cm^2 depth as a function of vertical cutoff rigidity R for various times in the solar cycle and Deep River Neutron Monitor (DRNM) count rates.

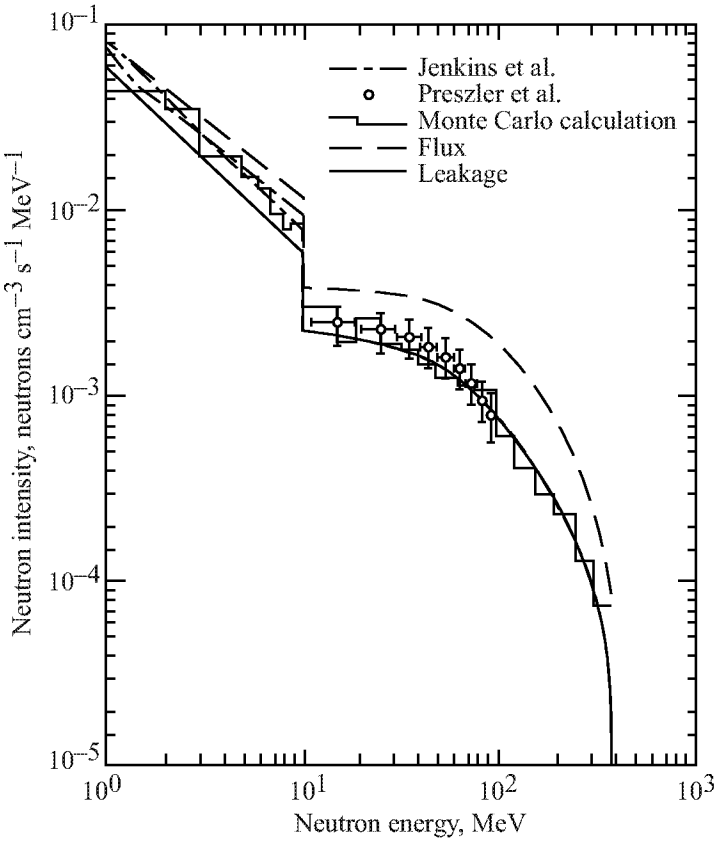

Figure 12. Neutron intensity at top of Earth's atmosphere over Palestine, TX during September 1971 according to various models and experiments.

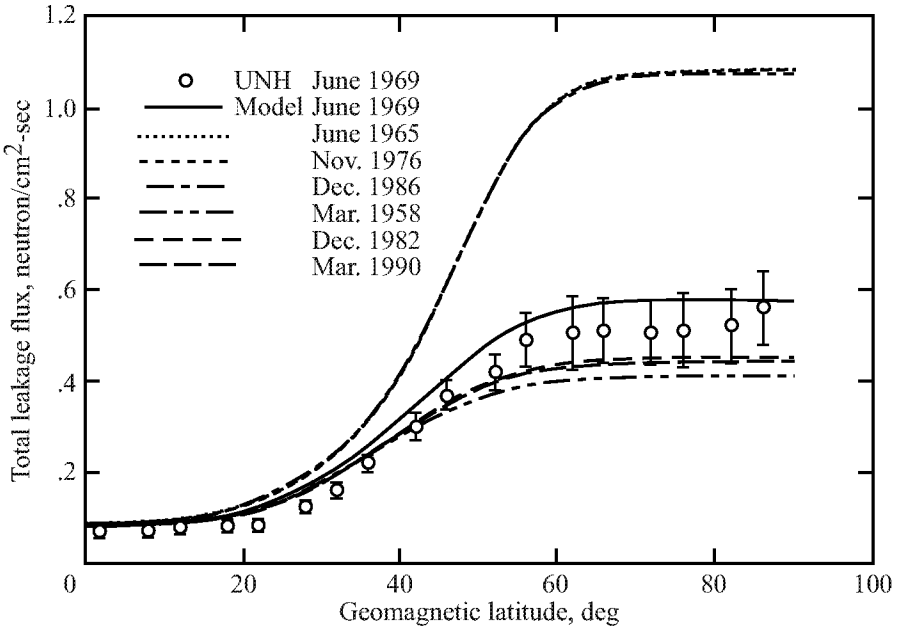

Figure 13. GCR induced neutron leakage flux for different solar cycle maxima and minima compared to measurements by University of New Hampshire by Lockwood et al.

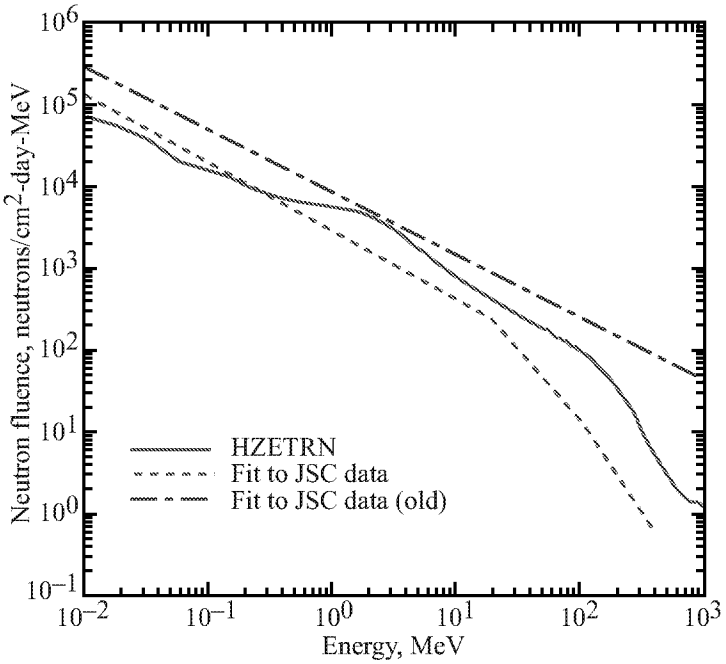

Figure 14. The neutron environment of STS-36 (62° inclination, 246 km) on Feb. 28–Mar. 3, 1990 predicted by current model compared to Johnson Space Center (JSC) data (Keith et al. 1992).

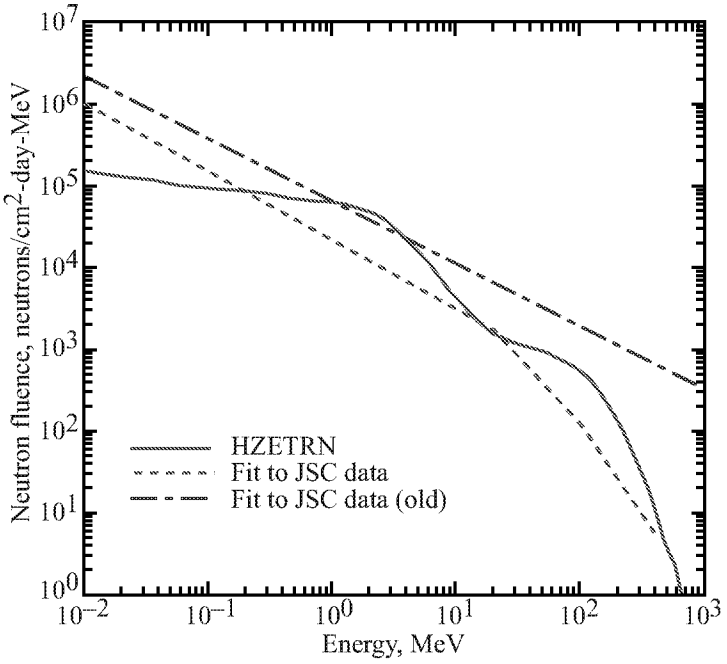

Figure 15. The neutron environment of STS-31 (28.5° inclination, 617 km) on Apr. 24–29, 1990 predicted by current model compared to JSC data (Keith et al. 1992).

REPORT DOCUMENTATION PAGE

Form Approved
OMB No. 0704-0188

1. AGENCY USE ONLY *(Leave blank)*	2. REPORT DATE	3. REPORT TYPE AND DATES COVERED
	May 2002	Technical Memorandum

4. TITLE AND SUBTITLE
Natural and Induced Environment in Low Earth Orbit

5. FUNDING NUMBERS
WU 705-30-11-11

6. AUTHOR(S)
John W. Wilson, Francis F. Badavi, Myung-Hee Y. Kim, Martha S. Clowdsley, John H. Heinbockel, Francis A. Cucinotta, Gautam D. Badhwar, William Atwell, and Stuart L. Huston

7. PERFORMING ORGANIZATION NAME(S) AND ADDRESS(ES)
NASA Langley Research Center
Hampton, VA 23681-2199

8. PERFORMING ORGANIZATION REPORT NUMBER
L-18165

9. SPONSORING/MONITORING AGENCY NAME(S) AND ADDRESS(ES)
National Aeronautics and Space Administration
Washington, DC 20546-0001

10. SPONSORING/MONITORING AGENCY REPORT NUMBER
NASA/TM-2002-211668

11. SUPPLEMENTARY NOTES
Wilson: Langley Research Center, Hampton, VA; Badavi: Christopher Newport University, Newport News, VA; Kim: College of William and Mary, Williamsburg, VA; Clowdsley and Heinbockel: Old Dominion University, Norfolk, VA; Cucinotta, and Badhwar: Johnson Space Center, Houston, TX; Atwell: Boeing Company, Houston, TX; Huston: Boeing Company, Huntington Beach, CA

12a. DISTRIBUTION/AVAILABILITY STATEMENT
Unclassified—Unlimited
Subject Category 93 Distribution: Standard
Availability: NASA CASI (301) 621-0390

12b. DISTRIBUTION CODE

13. ABSTRACT *(Maximum 200 words)*

The long-term exposure of astronauts on the developing International Space Station (ISS) requires an accurate knowledge of the internal exposure environment for human risk assessment and other onboard processes. The natural environment is moderated by the solar wind which varies over the solar cycle. The neutron environment within the Shuttle in low Earth orbit has two sources. A time dependent model for the ambient environment is used to evaluate the natural and induced environment. The induced neutron environment is evaluated using measurements on STS-31 and STS-36 near the 1990 solar maximum.

14. SUBJECT TERMS
Space radiation; Neutrons; Solar cycle; Low Earth orbit; STAR 93

15. NUMBER OF PAGES
26

16. PRICE CODE

17. SECURITY CLASSIFICATION OF REPORT	18. SECURITY CLASSIFICATION OF THIS PAGE	19. SECURITY CLASSIFICATION OF ABSTRACT	20. LIMITATION OF ABSTRACT
Unclassified	Unclassified	Unclassified	UL